

Higher-order Proton Cumulants in Au+Au Collisions at $\sqrt{s_{\text{NN}}} = 3$ GeV from RHIC-STAR*

YU ZHANG
FOR THE STAR COLLABORATION

yuz@cnu.edu.cn

Key Laboratory of Quark & Lepton Physics (MOE) and Institute of Particle Physics, Central China Normal University, Wuhan, 430079, China

Received August 12, 2022

In these proceedings, we present the higher-order cumulants of proton multiplicity distributions of the fixed-target (FXT) run in Au+Au collisions at $\sqrt{s_{\text{NN}}} = 3.0$ GeV. The cumulant ratios are presented as a function of centrality and collision energy. The proton cumulant ratio C_4/C_2 is consistent with fluctuations driven by baryon number conservation and indicates an energy regime dominated by hadronic interactions. These data imply that the QCD critical point could exist at energies higher than 3 GeV if created in heavy-ion collisions.

1. Introduction

Experimental evidences [1] at RHIC and the LHC have demonstrated the formation of Quark-Gluon Plasma (QGP) in ultra-relativistic heavy-ion collisions at small baryon chemical potential ($\mu_B \approx 0$ MeV) where the phase transition from the hadronic matter to QGP is suggested to be a crossover from state-of-the-art Lattice QCD calculations [2]. It has been conjectured that there is a first-order phase transition and a QCD critical point at the finite μ_B region in the QCD phase diagram. In the search for the possible QCD critical point, higher-order cumulants of conserved quantities such as net-baryon number, net-strangeness number, and net-charge number are sensitive observables to locate its position [3, 4, 5, 6]. Experimentally net-proton and net-kaon numbers are used as a proxy for net-baryon and net-strangeness numbers due to the difficulty to detect neutral particles in the experiment. Recent results from the STAR experiment on net-proton fourth-order cumulant ratio have shown intriguing non-monotonic energy

* Presented at Quark Matter 2022, Karkow, Poland, April 4-10, 2022

dependence with 3.1σ significance in the most central Au+Au collisions at $\sqrt{s_{\text{NN}}} = 7.7 - 200$ GeV [7, 8] while there are still large statistical uncertainties for energy $\sqrt{s_{\text{NN}}} < 19.6$ GeV. These proceedings reports proton cumulants and cumulant ratios up to 4th-order in $\sqrt{s_{\text{NN}}} = 3$ GeV Au+Au collisions from the STAR fixed-target experiment. The relevant analysis details and correction methods will also be shortly discussed. To understand the collision dynamics in the absence of the critical behavior, we have carried out simulations with a microscopic transport model UrQMD [9] for Au+Au collisions at $\sqrt{s_{\text{NN}}} = 3$ GeV. Connections between experimental data and physics implications in the high baryon density region will be discussed.

2. Experimental Observables

This section shows the definitions of cumulants and cumulant ratios. Let N represent net-proton number. The deviation from its mean value ($\langle N \rangle$) is defined as $\delta N = N - \langle N \rangle$. Then cumulants up to 4th-order can be written as:

$$\begin{aligned} C_1 &= \langle N \rangle, C_2 = \langle (\delta N)^2 \rangle, C_3 = \langle (\delta N)^3 \rangle, \\ C_4 &= \langle (\delta N)^4 \rangle - 3\langle (\delta N)^2 \rangle^2. \end{aligned} \quad (1)$$

The cumulants are related to the various moments as

$$M = C_1, \quad \sigma^2 = C_2, \quad S = \frac{C_3}{(C_2)^{3/2}}, \quad \kappa = \frac{C_4}{C_2^2}, \quad (2)$$

where M , σ^2 , S , and κ are mean, variance, skewness, and kurtosis, respectively. Various cumulant ratios like C_2/C_1 , C_3/C_2 , and C_4/C_2 are constructed to cancel volume dependence:

$$\frac{C_2}{C_1} = \sigma^2/M, \quad \frac{C_3}{C_2} = S\sigma, \quad \frac{C_4}{C_2} = \kappa\sigma^2. \quad (3)$$

3. Analysis Details

The analysis used around 140 million $\sqrt{s_{\text{NN}}} = 3$ GeV Au+Au collisions events which are collected by the dedicated physics fixed-target run of the STAR experiment in the year 2018. The centrality is determined using charged particle reference multiplicity excluding protons and light nuclei within $-2 < \eta < 0$ where η is pseudo-rapidity in the lab frame. As shown in Fig. 1 protons are identified by comparing the energy loss measured by the Time Projection Chamber (TPC) with theoretical predictions (Fig. 1(a)). At high momentum ($p_{\text{lab}} > 2$ GeV/c), due to the contamination from other particles, the mass square measured by Time of Flight (TOF) is used to

ensure proton purity (Fig. 1(b)). The anti-protons are negligible ($\bar{p}/p < 10^{-6}$) at $\sqrt{s_{\text{NN}}} = 3$ GeV thus the proton cumulants are measured in the analysis. Figure 1(c) shows proton acceptance with the combination of TPC and TOF. The red dashed box indicates the acceptance window used in this analysis.

Cumulants are corrected for detector efficiencies by a track-by-track method [10, 11]. The rapidity (y) and transverse-momentum (p_{T}) dependences of detector efficiency are considered. To correct the pileup effect due to the finite thickness of the gold target, a pileup correction method [12, 13] is used. As seen in our model simulation, there is a large initial volume fluctuation effect when calculating cumulants at $\sqrt{s_{\text{NN}}} = 3$ GeV, thus we tested an initial volume fluctuation correction method [14]. We measured cumulants as a function of reference multiplicity, and then obtained centrality binned results by the Centrality Bin Width Correction (CBWC) [15]. The statistical uncertainties of cumulants are estimated by the bootstrap method. The systematic uncertainties are estimated by varying analysis cuts related to centrality, pileup effect, track quality, and detector efficiency.

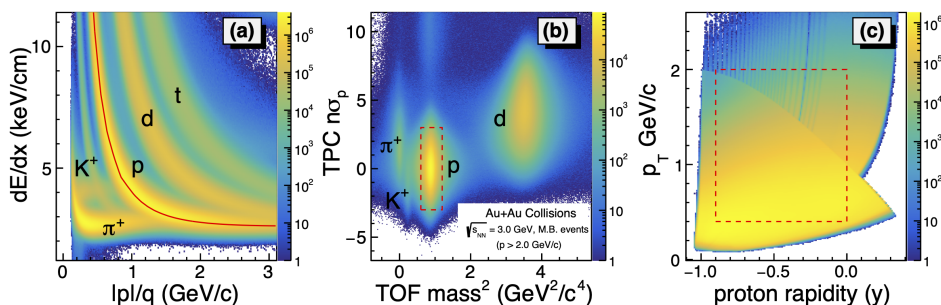


Fig. 1. Panel (a): TPC track energy loss (dE/dx (keV/cm)) vs. momentum; pion, kaon, deuteron and triton are labeled. The proton Bethe-Bloch curve is plotted with red line. Panel (b): TPC $n\sigma_p$ vs. TOF mass^2 . Panel (c): Transverse momentum (p_{T}) vs. proton rapidity.

4. Results

Figure 2 shows the centrality dependence of the proton cumulant ratios C_2/C_1 , C_3/C_2 , and C_4/C_2 within $-0.5 < y < 0$ and $0.4 < p_{\text{T}} < 2.0$ GeV/c. The 3 GeV data shown with black open squares are corrected for detector efficiency and pileup effect and then the CBWC was applied to obtain centrality binned results. The red circles and blue triangles are additionally

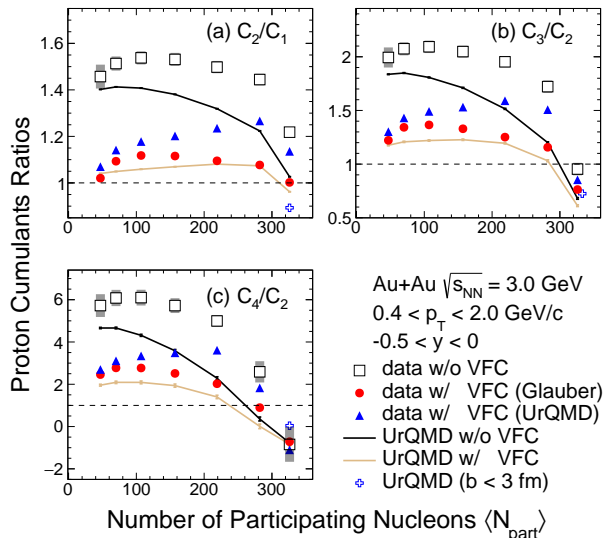


Fig. 2. Centrality dependence of proton cumulants and cumulant ratios up to 4th-order in Au+Au collisions at $\sqrt{s_{\text{NN}}} = 3$ GeV within kinematic acceptance $-0.5 < y < 0$ and $0.4 < p_{\text{T}} < 2.0$ GeV/c. The black squares are results without volume correction while red circles and blue triangles represent results with volume correction using Glauber and UrQMD model, respectively.

corrected for initial volume fluctuation using Glauber and UrQMD models, respectively. It is clear that the volume fluctuation correction shows a strong model dependence and affects the centrality dependence, particularly in peripheral collisions. The respective dynamics in the UrQMD and Glauber model for charged hadron production lead to two different mappings from the measured final charged hadron multiplicity distributions to the initial geometry. This difference is likely to be the dominant source of the model dependence in the VFC. On the other hand, one can see in the figure that the difference between results with and without the VFC is small for higher order ratios C_3/C_2 and C_4/C_2 in the most central bin.

Figure 3 shows the collision energy dependence of cumulant ratio C_4/C_2 of net-proton and proton multiplicity distributions in central Au+Au collisions [16]. As reported in Refs. [8, 7] the net-proton and proton C_4/C_2 show a non-monotonic energy trend in central Au+Au collisions. A minimum is seen at around $\sqrt{s_{\text{NN}}} = 20$ GeV and then C_4/C_2 becomes close to unity with large statistical uncertainty when decreasing collision energy. The new measurement of proton C_4/C_2 for $\sqrt{s_{\text{NN}}} = 3$ GeV central Au+Au

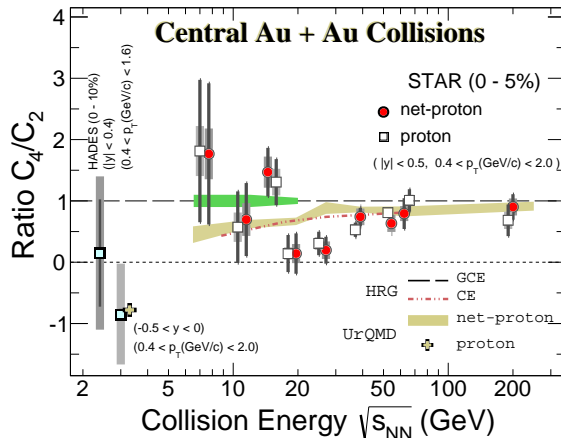


Fig. 3. Collision energy dependence of cumulants ratio C_4/C_2 in central Au+Au collisions within kinematic acceptance cut $0.4 < p_T < 2.0$ GeV/c. UrQMD calculations are shown with gold band for net-proton with rapidity cut $|y| < 0.5$ and gold filled cross for proton with rapidity cut $-0.5 < y < 0$. Statistical and systematic uncertainty are shown with black and grey bars, respectively. The green shaded area indicates the projected statistical uncertainty with BES-II data.

collisions is around -1, which is reproduced by the hadronic transport model UrQMD while at higher energies the non-monotonic energy dependence is not reproduced by various non-critical models including the UrQMD and HRG [17] models. Precision data in the energy window of $3 < \sqrt{s_{NN}} < 20$ GeV are needed in order to explore the possibility of critical phenomena. The HADES collaboration has reported the proton cumulant ratio in $\sqrt{s_{NN}} = 2.4$ GeV Au+Au collisions within acceptance window $0.4 < p_T < 1.6$ GeV/c and $|y| < 0.4$: $C_4/C_2 = 0.15 \pm 0.9$ (stat.) ± 1.4 (sys.) [18] which is consistent with 3 GeV result within uncertainty although detailed comparison should be done within same acceptance.

5. Summary

In this paper, we reported cumulant ratios of proton multiplicity distributions in $\sqrt{s_{NN}} = 3$ GeV Au+Au collisions by the STAR fixed-target experiment. The proton C_4/C_2 is observed to be -0.85 ± 0.09 (stat.) ± 0.82 (sys.) in the most central 0-5% centrality at $\sqrt{s_{NN}} = 3$ GeV. Compared to higher energy results and the transport model calculations, the suppression in C_4/C_2 is consistent with fluctuations driven by baryon number conser-

vation and indicates an energy regime dominated by hadronic interactions, which implies that the QCD critical point could exist at energies higher than 3 GeV if discovered in heavy-ion collisions. New data sets have been collected during the second phase of the RHIC beam energy scan program for Au+Au collisions at $\sqrt{s_{NN}} = 3 - 19.6$ GeV. The analysis on those datasets will be crucial in exploring the QCD phase structure at high baryon density region and locating the critical point.

Acknowledgments

This work was supported by the National Key Research and Development Program of China (Grant No. 2020YFE0202002 and 2018YFE0205201), the National Natural Science Foundation of China (Grant No. 12122505 and 11890711) and the Fundamental Research Funds for the Central Universities(CCNU220N003).

REFERENCES

- [1] J. Adams et al. (STAR) *Nucl. Phys. A*, 757:102–183, 2005.
- [2] Y. Aoki et al. *Nature*, 443:675–678, 2006.
- [3] M. A. Stephanov. *Phys. Rev. Lett.*, 102:032301, 2009.
- [4] M. Asakawa, S. Ejiri, and M. Kitazawa. *Phys. Rev. Lett.*, 103:262301, 2009.
- [5] X. Luo and N. Xu. *Nucl. Sci. Tech.*, 28(8):112, 2017.
- [6] S. Gupta et al. *Science*, 332:1525–1528, 2011.
- [7] J. Adam et al. (STAR) *Phys. Rev. Lett.*, 126(9):092301, 2021.
- [8] M. Abdallah et al. (STAR) *Phys. Rev. C*, 104(2):024902, 2021.
- [9] M. Bleicher et al. *J. Phys. G*, 25:1859–1896, 1999.
- [10] T. Nonaka, M. Kitazawa, and S. Esumi. *Phys. Rev. C*, 95(6):064912, 2017. [Erratum: *Phys.Rev.C* 103, 029901 (2021)].
- [11] X. Luo and T. Nonaka. *Phys. Rev. C*, 99(4):044917, 2019.
- [12] T. Nonaka, M. Kitazawa, and S. Esumi. *Nucl. Instrum. Meth. A*, 984:164632, 2020.
- [13] Y. Zhang, Y. Huang, T. Nonaka, and X. Luo. *Nucl. Instrum. Meth. A*, 1026:166246, 8 2021.
- [14] P. Braun-Munzinger, A. Rustamov, and J. Stachel. *Nucl. Phys. A*, 960:114–130, 2017.
- [15] X. Luo, J. Xu, B. Mohanty, and N. Xu. *J. Phys. G*, 40:105104, 2013.
- [16] M. S. Abdallah et al. (STAR) *Phys. Rev. Lett.*, 128(20):202303, 2022.
- [17] P. Garg et al. *Phys. Lett. B*, 726:691–696, 2013.
- [18] J. Adamczewski-Musch et al. (HADES) *Phys. Rev. C*, 102(2):024914, 2020.